Catal Lett (2017) 147:1485–1495
DOI 10.1007/s10562-017-2056-y

Solid Acidic NbO_x/ZrO_2 Catalysts for Transformation of Cellulose to Glucose and 5-Hydroxymethylfurfural in Pure Hot Water

Nikolay V. Gromov[1,2] · Oxana P. Taran[1,2] · Viktoria S. Semeykina[1,3] · Irina G. Danilova[1] · Andrey V. Pestunov[4] · Ekaterina V. Parkhomchuk[1,3] · Valentin N. Parmon[1,3]

Received: 25 December 2015 / Accepted: 13 April 2017 / Published online: 27 April 2017

Abstract Solid acid NbO_x/ZrO_2 catalysts containing 0, 0.5, 1.1 and 2.8 wt.% of Nb were prepared for one–pot hydrolysis-dehydration of mechanically activated cellulose in pure hot water to produce glucose and 5-hydroxymethylfurfural. The catalysts were characterized (XRD, N_2 adsorption, ICP-OES, UV–Vis DRS) and tested in cellulose processing at 453 K. The catalytic activity increased as follows: $0.5\%Nb/ZrO_2 < ZrO_2 << 1.1\%Nb/ZrO_2 \sim 2.8\%Nb/ZrO_2$. This series was accounted for by the acid-basic properties of ZrO_2, by the inhibition of its active sites by monomer niobium species and by the appearance of Brønsted acidity upon the formation of NbO_x-containing polymer structures. The highest glucose and 5-HMF yields (22 and 16 mol%, respectively) were achieved over $2.8\%Nb/ZrO_2$.

✉ Oxana P. Taran
oxanap@catalysis.ru

[1] Boreskov Institute of Catalysis SB RAS, Akad. Lavrentiev Av., 5, Novosibirsk 630090, Russia

[2] Novosibirsk State Technical University, Karl Marx Av., 20, Novosibirsk 630073, Russia

[3] Novosibirsk State University, Pirogova St., 2, Novosibirsk 630090, Russia

[4] Institute of Chemistry and Chemical Technology SB RAS, Akademgorodok, 50, Krasnoyarsk 660036, Russia

Graphical Abstract

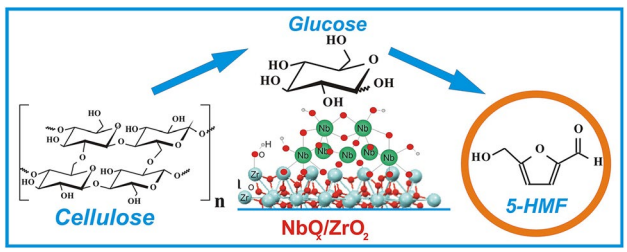

Keywords Cellulose · Glucose · 5-Hydrohymethylfurfural · Niobium oxide · Zirconia · Hydrolysis-dehydration

List of Symbols

C	Concentration, mol L^{-1} or g L^{-1}
CI	Crystalline index, %
CSR	Coherent-scattering region, nm
$<d_l>$	Average length of cellulose particles, μm
$<d_{PORE}>$	Average diameter of catalyst pores, nm
E_g	Edge energy, eV
m	Mass, g
M	Molar mass, g mol^{-1}
N	Number of atoms
n_{Cell}	Amount of carbon in cellulose sample, mol
R	Initial rate of formatting the main reaction products (glucose + 5-HMF), mol L^{-1} s^{-1}
TOF	Turnover frequency, s^{-1}
T	Temperature, K
V	Volume, L
V_{PORE}	Volume of the pores in a catalyst structure, cm^2 g^{-1}
S_{BET}	Specific surface area, m^2 g^{-1}
X	Conversion, %

Y	Yield, %
Y_{Σ}	Total yield, %

Abbreviations

Cell	Cellulose
Glu	Glucose
FA	Formic acid
Fru	Fructose
Fur	Furfural
5-HMF	5-Hydroximethylfurfural
K_w	Ion product of water
LA	Levulinic acid
wt	Weight

Greek Symbols

ω	Mass portion
τ	Time, h or s

1 Introduction

The depletion of high-quality fossil fuels, shortage of food raw materials, and increasing emission of CO_2 make it of urgent importance to develop new catalytic technologies for production of organic compounds from alternative raw materials [1–5]. Glucose is an industrially important valuable carbohydrate produced traditionally by enzymatic or acid hydrolysis of starch or sucrose. 5-Hydroximethylfurfural (5-HMF) known as a platform molecule is a promising agent for chemical industry, manufacturing plastics and fuel production [1, 5–13]. 5-HMF can be quite easily prepared from hexoses such as glucose and fructose [1, 8, 11, 12, 14, 15] which are the products of hydrolytic processing of di- and/or polysaccharides (sucrose, starch, inulin) derived from edible sources (crops and vegetables). A high selectivity (up to 89%) to 5-HMF can be archived by treating fructose in biphasic systems comprising dilute aqueous solution of mineral acids, inorganic salts and organic solvents (DMSO, MIBK, THF, alcohols, ketones etc.) [16–19]. Substitution of solid acid catalyst (silicoaluminophosphate SAPO-44) for mineral acids provides high yields of 5-HMF from fructose (78%), glucose (67%), maltose (57%), cellobiose (56%) and starch (68%) [20]. Different catalytic systems with ionic liquids as solvents were used to produce 5-HMF at high yields from fructose (75–92%) [19, 21, 22], glucose (up to 88%) [23] and sucrose (48%) [21]. An only commercial technology is currently on stream for the production of 5-HMF from fructose using a modified hydrothermal carbonization process [24]. AVA Biochem, Switzerland, has started the industrial manufacturing of 5-HMF since January 2014 [25]. The involved compounds are important for the food industry and, hence, there may occur undesirable competition for agricultural lands and resources. Cellulose is the main component of plant biomass and the most abundant natural non-food polysaccharide [2, 26]. On the other hand, organic solvents or ionic liquids are more expensive and ecologically unfavorable than water as the solvent. Therefore transformation of cellulose in pure hot water over a solid acid catalyst seems the most attractive alternative for one-pot catalytic production of glucose and 5-HMF without isolation of intermediates [8, 9, 27].

A number of catalysts such as soluble mineral acids and bases [28], heteropolyacids [29], carbons with different morphology [30], supported noble metals [31], polymer resins [32], alumina and silica [32–35], zeolites [34, 36] were suggested for cellulose depolymerization in aqueous solutions. However, there are some drawbacks of these catalysts. For example, soluble catalysts (mineral acids, bases, heteropolyacids) are corrosion-active and needs separation from soluble products. Noble metals are quite expensive. The catalysts based on carbons and silica may be unstable in aggressive hot water. It is important to emphasize that the authors of works cited above usually do not report explicit data on 5-HMF yield but pay only attention to the glucose formation. Hence, the development of highly active and stable solid acid catalyst for the one-pot hydrolysis-dehydration of cellulose to glucose and 5-HMF is still a great challenge [37].

Oxides of niobium(V), titanium(IV), zirconium(IV), tungsten(VI), aluminum(III) possessing acid or acid-base properties are stable in hot water and seem the most promising solid catalysts. These oxides were successfully applied for hydrolysis of some disaccharides (cellobiose, sucrose, maltose) [38–40] and dehydration of monosaccharides (fructose, glucose) to 5-HMF [41–44]. ZrO_2 also was tested as a catalyst for transformation of saccharides into 5-HMF. Zirconia was active to isomerization of glucose to fructose [43, 45] and to glucose dehydration into 5-HMF [45, 46]. The highest yields of 5-HMF from fructose were 38% using microwave heating and only 12% using sand bath heating [43].

However, the application of the said metal oxides as catalysts for direct hydrolytic-dehydration of cellulose is only discussed in few papers (see, e.g., reviews [8, 12, 27, 47]). The possibility of direct processing biomass or cellulose into 5-HMF over modified zirconia catalysts such as ZrO_2–TiO_2 and silica-zirconia cogel SiO_4–ZrO_2 was shown elsewhere [46, 48]. Chareonlimkun and co-authors reported 8.6% yield of 5-HMF from different biomass species (sugarcane bagasse, rice husk and corncob) over ZrO_2–TiO_2 at 573 K [46]. Gliozzi et al. produced 5-HMF and furfural from softwood dust at the total yield of 8.2% over silica-zirconia at 423 K [48]. However, pure oxides ZrO_2, SiO_2 are low active to cellulose hydrolysis [32, 33]. Hydrolysis can be improved by anchoring sulfuric acid species onto ZrO_2

[32, 49], TiO_2 [50], SiO_2 [51]. Niobium oxide is another promising catalyst for hydrolysis processes [52] including hydrolysis of soluble disaccharides [39, 53] and for dehydration of monosaccharides into 5-HMF [42, 44, 53]. Niobium oxide bears a great array of acidic centers on the surface and seems very promising additive to ZrO_2. Niobium oxide supported on zirconia and zirconium-niobium mixed oxides catalyzed successfully dehydration of 2-prapanol [54], glycerol [55] and 1,2-propanediol [56] due to Brønsted acidity of polymeric niobium oxide species.

The aim of the present work was to develop a solid acid catalytic system containing niobium oxide supported on ZrO_2 for one-pot hydrothermal processing of cellulose to produce glucose and especially 5-HMF in pure hot water as well as to explore a promoting effect of niobium on catalyst activity.

2 Experimental

2.1 Chemicals and Materials

Isopropoxide of zirconium $Zr(OiPr)_4$ (70 vol% solution in iPrOH, Acrosorganics) and hydrate of niobium(V) oxalate $C_{10}H_5NbO_{20}{\cdot}xH_2O$ (Alfa Aesar) were used for catalyst synthesis. Microcrystalline cellulose (fraction <0.10 mm, Vekton, Saint-Petersburg, Russia) was used as the substrate. 5-Hydoxymethylfurfural (Sigma-Aldrich), D-fructose (Sigma-Aldrich), D-mannose (Sigma-Aldrich), D-glucose (Reahim, Moscow, Russia), D-cellobiose (Alfa Aesar), levulinic acid (Acros Organics) were purchased as HPLC standards. Milli-Q water (Millipore, France) was used for preparing all the solutions.

2.2 Catalyst Preparation and Characterization

Zirconia was prepared by diluting 5 mL of $Zr(O^iPr)_4$ solution (70% solution in ^{i}PrOH, Acros organics) with 5 mL of ^{i}PrOH. The reaction solution was hydrolyzed by water steam and calcined for 8 h at 873 K (heating rate 2.5 K min^{-1}).

For supporting niobium oxide, zirconia powder was mounted into a thermostated reactor and vacuumized at 323 K for 15 min. The calculated amount of niobium(V) oxalate was dissolved in a small volume of distilled water and placed into the thermostated reactor containing ZrO_2. The catalyst was kept in the reactor for 30 min, dried in air for 24 h, and calcined at 723 K for 4 h (heating rate 3.6 K min^{-1}).

Textures catalysts and the zirconia support were characterized using low-temperature nitrogen absorption at 77 K on ASAP-2400 device (Micromeritics, USA). All the catalysts were vacuumized to reach pressure of 6 Torr at 473–573 K before the analysis. The BET specific surface areas (S_{BET}) were calculated from the adsorption curves of the isotherms. Pore volumes were determined by the α_S-method, and pore size distribution by the BJH method.

The contents of Nb in the catalysts before and after the experiments as well as in the reaction media were measured by ICP-OES with Optima 4300 DV spectrophotometer (PerkinElmer Inc., USA).

XRD studies of the catalysts were conducted using BrukerD8 Advabced (Germany) diffractometer (step $2\Theta = 0.05°$, signal accumulation time 1–3 s per point). Monochromatic CuKα-radiation ($\lambda = 1.5418$ Å) was used for recording spectra. The phase composition was analyzed using ICSD data base (2009). Theoretical XRD patterns were calculated and phase compositions estimated using the PowderCell 2.3 program package.

UV–Vis diffuse reflectance spectra (UV–Vis DRS) of the catalysts without any pretreatment were acquired at ambient temperature using UV-2501 PC Shimadzu spectrometer with a IRS-250A diffusion reflection attachment at the 11,000–54,000 cm^{-1} range using $BaSO_4$ as the reference. The UV–Vis edge energy (E_g) was determined from the intercept of the straight line of the low-energy rise at the plot of $[F(R_\infty)h\nu]^2$ versus $h\nu$, where $h\nu$ is the incident photon energy [57].

2.3 Cellulose Mechanical Activation and Characterization

A planetary-type mill Pulverizette 5 (Fristch, Germany) was used for mechanical activation of cellulose. Activation conditions: drum volume 250 mL, cellulose mill feeding 15 g, ball diameter 20 mm, ball feeding 7 pcs., activation time 40 min.

Cellulose particle size was determined by optical microscope Zeiss—Axiostar plus (Germany) equipped with a photocamera. The average diameter of cellulose particles was calculated as the mean diameters of 100 particles.

XRD studies of cellulose samples were carried out with BrukerD8 Advabced (Germany) diffractometer with monochromatic CuKα-radiation ($\lambda = 1.5418$ Å) at the 2θ range of 10°–40°. All the diffraction patterns were distributed into individual peaks (101, 10$\bar{1}$, 021, 002, 040 and amorphous cellulose) with 2θ equal to 15.2, 16.8, 20.6, 22.7, 34.1 and 21.5, respectively [58]. Crystallinity index (CI) was evaluated as the relation of the sum of 101, 10$\bar{1}$, 021, 002, 040 peak squares subtracting the square of amorphous cellulose halo ($2\theta \sim 21.5°$) to the total square of diffraction pattern ($2\theta = 10°$–$40°$) [59]. The coherent scattering region (CSR) was determined by the Seliakov–Sherrer formula [60].

2.4 Catalytic Tests and Analytic Techniques

Cellulose hydrolysis-dehydration was carried out in an autoclave (Autoclave Engineers, USA) at 453 K, argon pressure 1 MPa under intensive stirring at 1500 rpm. Cellulose and a catalyst (10 g L^{-1} each) and 45 mL of distilled water were put into the reactor. The reactor was purged with flowing argon, heated up to 453 K, and the reaction was started. In 0, 1, 2, 3 and 5 h of the reaction, aliquots of the reaction mixture (~1 mL) were drawn from the reactor to monitor the concentrations by HPLC; these aliquot quantities did not influence the process in the autoclave.

The samples were analyzed using Shimadzu Prominence LC-20 HPLC equipped with a RI detector. Saccharides and acids was analyzed using Rezex RPM-Monosaccharide Pb^{2+} or Rezex ROA-Organic Acids columns (Phenomenex, 300×5.0 mm) termostated at 343 and 313 K, respectively. Deionized water or 1.25 mM H_2SO_4 solution were used at the flow rate of 0.6 mL min^{-1} for analysis of sugar and acid, respectively.

The total organic carbon (TOC) content was determined after the reaction using Multi N/C 2100S TOC Analyzer (Analytik Jena, Germany). A 500 µL aliquot of the reaction mixture was added into an analyzer injector. Time of analysis was min. The amount of organic carbon (g L^{-1}) was calculated based on the calibration curves plotted before.

pH of the reaction solutions was measured before and after the experiment with a pH tester Anion 4100 (TD Anion, Russia).

3 Results and Discussion

3.1 Cellulose Pretreatment

Cellulose is a biopolymer which consists of chains with glucose monomer residues linked by 1,4-glycosidic bonds. Side hydroxyl groups in the polymer chains form intramolecular (between residues of a chain) and intermolecular (between chains) hydrogen bonds. The hydrogen bonding leads to the ordering of cellulose chains and to the formation of crystal structure [61]. While crystalline cellulose is resistant to chemical transformations [62], its activation is an indispensable procedure.

In this study cellulose was activated by grinding in a planetary mill. This method seems quite promising because of amorphizating crystal domains and cleavage of glycosidic and hydrogen bonds [61, 63]. Optical spectroscopic studies of cellulose particles before and after the activation revealed that the average length decreased from 114±35 (Fig. 1a) to 13±6 µm (Fig. 1b). Comparison of optical and SEM images of particles related to initial and activated cellulose showed changes in the particle shape from oblong to almost spherical crystals (Fig. 1). XRD pattern with reflexes typical of the crystalline cellulose, CSR ranging from 4 to 7 nm and calculated CI equal to 80–90% were observed for the initial microcrystalline cellulose. Grinding cellulose during 40 min led to a considerable increase in the amorphous halo (2θ ~ 21.5°) on the XRD pattern with simultaneous decrease in CI (35–55%) and CSR (2–4 nm) (Table 1).

3.2 Catalysts Preparation and Characterization

Zirconia (ZrO_2) was prepared by hydrolysis of $Zr(O^iPr)_4$ in water stream followed by calcination at 873 K. Niobium oxide (0.5, 1.1 and 2.8 wt.%) was supported on zirconia (see Sect. 2.2). The loading of Nb impregnated into the samples was determined by elemental ICP-OES analysis of the fresh catalysts. Analysis of the spent catalysts and solutions after the reaction indicated no leaching of Nb during the reaction in the hydrothermal reaction media.

Texture properties of the catalysts were revealed by low-temperature nitrogen adsorption (Table 2). Specific surface area (S_{BET}) of non-modified ZrO_2 was 16 m^2 g^{-1}, and total pore volume (V_{PORE}) was extremely low. The type III isotherms have been identified which are typical of non-porous and/or macroporous materials free of micro/mesopores. While S_{BET} for this kind materials often are no more than 10–20 m^2 g^{-1} because of agglomeration during the calcination [64], low S_{BET} of ZrO_2 was expected. Addition of niobium oxide to the catalyst makes S_{BET} decreased by ~25% to 11–12 m^2 g^{-1} and the average pore diameter ($<d_{PORE}>$) increased by 50% from 20 to 30 nm at the constant V_{PORE}. S_{BET} and $<d_{PORE}>$ do not depend on the Nb loading in the catalysts in the range of 0.5–2.8 wt.%.

The nominal monolayer coverage was calculated using the textural data in the assumption that the cross-section of a Nb_2O_5 unit is 0.32 nm^2 [54, 65].

From XRD data, the ZrO_2 and NbO_x/ZrO_2 catalysts contain mainly monoclinic phase of zirconia (99% for pure ZrO_2 and 97% for NbO_x/ZrO_2) (Table 2). The monoclinic structure is more thermally stable then the tetragonal one. A decrease in the proportion of the monoclinic phase during deposition of niobium oxide on the ZrO_2 was reported elsewhere [56, 66]. We observed a similar trend. This observation allows us to conclude that the immobilization of Nb-containing particles stabilizes the tetragonal modification of zirconia. The obtained XRD data indicate the amorphous state of the active component but not the formation of crystalline niobium pentooxide (Fig. 2). The absence of crystalline phases of niobium pentooxide after its immobilization on the surface of other oxide supports was shown earlier [56].

The coordination geometry and the chemical arrangement of the Nb species in the catalysts were studied by

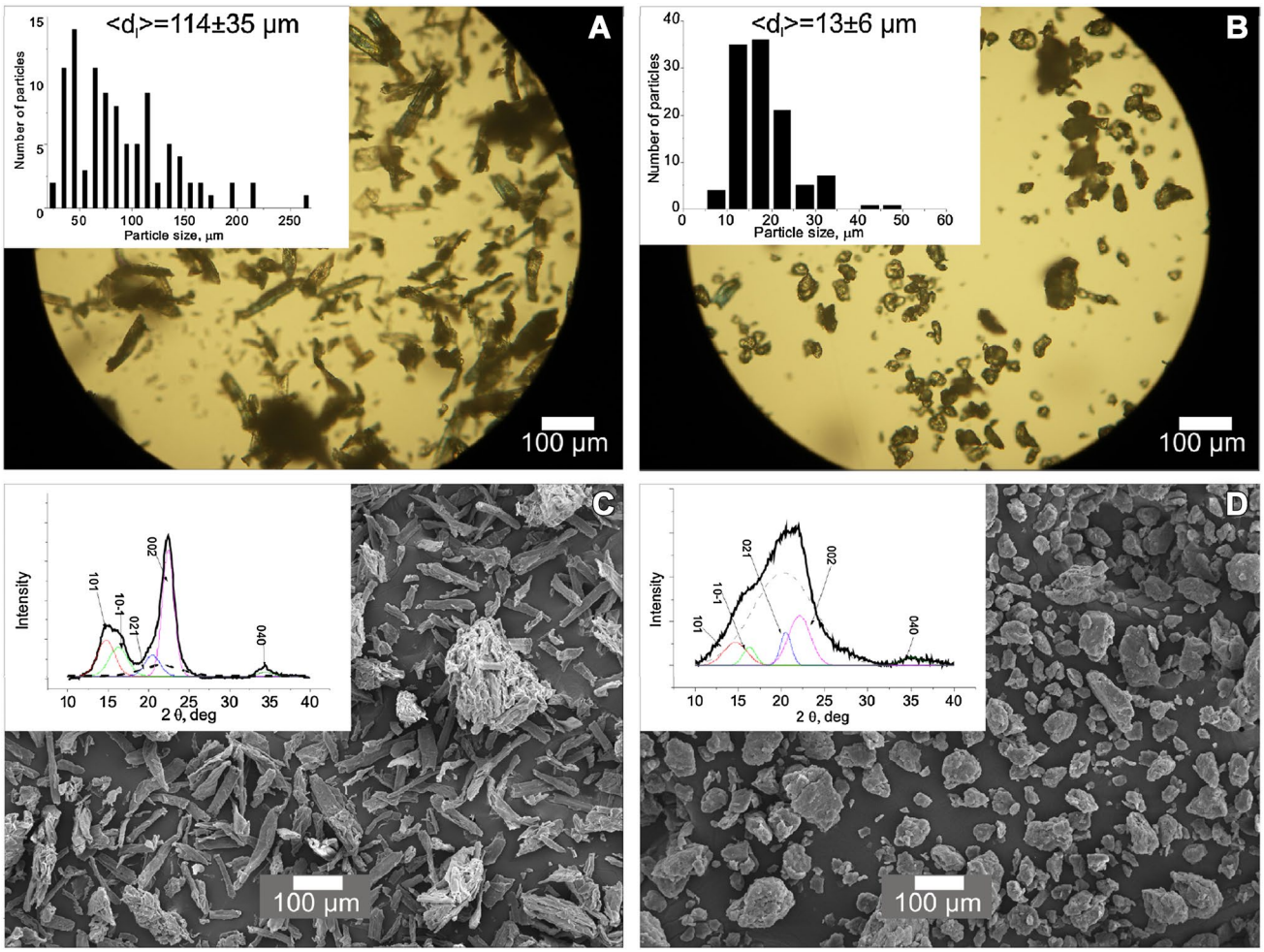

Fig. 1 Microphotographs and particle size distribution (*insets*) (**a, b**), SEM images and XRD pattern (*insets*) (**c, d**) for the non-treated microcrystalline cellulose (**a, c**) and the activated 40 min in planetary-mill cellulose (**b, d**)

Table 1 The parameters of cellulose samples before and after 2400 s (τ) ball-milling: average particle length $<d_l>$, crystalline index (CI), coherent-scattering region (CSR)

Sample	τ, s	Sample temperature during activation, K	$<d_l>$, μm	CI, %	CSR, nm
Cellulose before activation	0	–	114 ± 35	80–90	4–7
Activated cellulose	2400	~373	13 ± 6	35–55	2–4

Table 2 Texture parameters of NbO_x/ZrO_2 catalysts determined by nitrogen adsorption and ZrO_2 phase composition revealed by XRD

Sample	Texture parameters			Nb, atoms nm^{-2}	% of monolayer[a]	Phase composition ZrO_2, %	
	S_{BET}, $m^2\ g^{-1}$	V_{PORE}, $cm^3\ g^{-1}$	$<d_{PORE}>$, nm			Monoclinic	Tetragonal
ZrO_2	16	0.08	20	–	–	99	1
0.5%Nb/ZrO_2	12	0.09	30	2.7	40	97	3
1.1%Nb/ZrO_2	11	0.08	29	6.5	100	97	3
2.8%Nb/ZrO_2	12	0.09	29	15.1	240	97	3

[a]Theoretical value was estimated assuming that each Nb_2O_5 unit occupies a surface of 0.32 nm^2

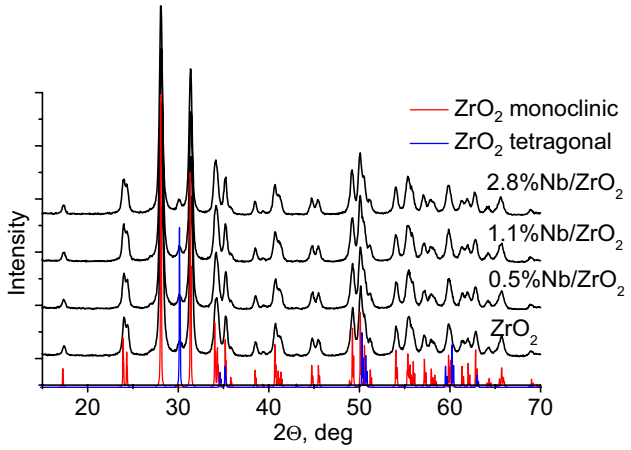

Fig. 2 XRD diffraction patterns of NbO_x/ZrO_2 catalysts

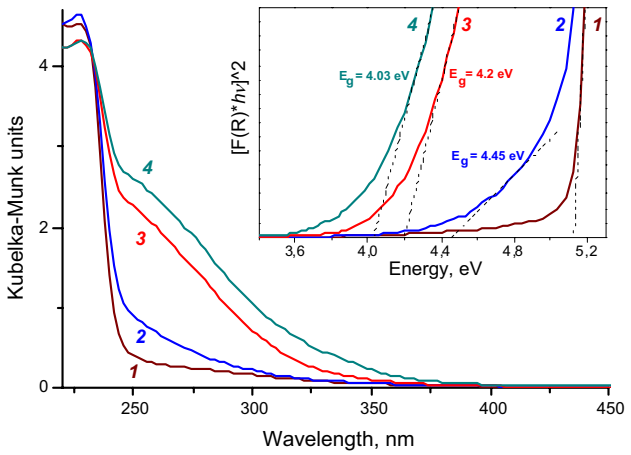

Fig. 3 Diffuse reflectance UV–Vis spectra of ZrO_2 (*1*) and NbO_x/ZrO_2 catalysts: 0.5 wt.% Nb (*2*), 1.1 wt.% Nb (*3*), 2.8 wt.% Nb (*4*); *inset* shows the Kubelka–Munk function versus energy of the excitation source

UV–Vis DRS spectroscopy (Fig. 3). It was shown [67] that the traditional method used to study Brønsted acid sites by NH_3 or pyridine adsorption followed by IR spectroscopy was low sensitive to the catalysts with the loading of niobium <5 wt.%. Therefore, we chose the UV–vis DRS spectroscopic technique the relationship between the absorption edge energy and the degree of condensation of niobium oxide species shown before [54, 68]. The zirconia absorption edge energy (E_g = 5.13 eV) is consistent with the reported data [54] due to the charge transfer $O^{2-} \rightarrow Zr^{4+}$. The absorption edge energy for Nb-containig species in NbO_x/ZrO_2 for 0.5%Nb/ZrO_2 (E_g = 4.45 eV) is close to that reported for isolated NbO_4 species in Nb-MCM-41 [68] and to that of niobium oxalate [54] that indicates the predominant formation of isolated NbO_4. The UV–vis absorption edge energy for 1.1%Nb/ZrO_2 and 2.8%Nb/ZrO_2 decreases to 4.20 and 4.03 eV (Fig. 3, *inset*) toward the value typical of polymer Nb structures (for example, niobic acid, $Nb_2O_5 \cdot nH_2O$, E_g = 3.9 eV [54]). However, these values remain higher than that of niobium oxide (E_g = 3.42–3.2 eV). The red shift of edge energy at an increase of the Nb loading indicates a higher degree of polymerization: the Nb cations in the 0.5%Nb/ZrO_2 sample are predominantly isolated NbO_4 species, while polymerized surface niobium oxide NbO_x (NbO_6) species are formed in the 1.1–2.8%Nb/ZrO_2 catalysts [54, 68]. These results are consistent with the nominal monolayer coverage assumed from the texture data (40% of monolayer for 0.5%Nb/ZrO_2; 100 and 240% for 1.1 and 2.8%Nb/ZrO_2, respectively). The acidity of our catalysts was confirmed indirectly by pH measuring.

3.3 Cellulose One-Pot Hydrothermal Hydrolysis-Dehydration

The results of the catalytic hydrothermal hydrolysis-dehydration of mechanically-activated cellulose in the autoclave at 453 K and inert argon atmosphere are shown in Table 3 and Fig. 4. The main reaction products were glucose and 5-HMF. The formation of low amounts of mannose and fructose (via glucose isomerization), formic and levulinic acids (caused by 5-HMF decomposition), and furfural (the side product of fructose transformation) were observed in this study and reported in literature [69, 70]. Oligosaccharides were formed during the 1st hour of the reaction, then the yields of soluble oligomers went down to zero. The formation of humins (brown colored side products of monosaccharide and 5-HMF condensation) also was observed under the reaction conditions. While both the formation of humans and cellulose transformations over solid catalysts need high temperature, and former are unavoidably produced. It has been shown before [71] that amorphous cellulose hydrolysis starts at 423 K and crystalline cellulose at 453 K. With our catalytic system comprising the solid substrate and the solid catalyst, the critical step is depolimerization of cellulose to soluble oligosaccharides to be transformed to glucose and 5-HMF over a catalyst. It is well known that dissociation constant of water (K_w) increases with temperature elevation. At 473 K $-\lg K_w$ becomes equal to 11 that leads to an increase in the concentrations of H^+ and OH^- ions [72]. The increase in $-\lg K_w$ allows water to behave as the co-catalyst during cellulose hydrolysis-dehydration [73].

The yields of the reaction products were calculated according to formula [74]:

$$Y = \frac{C \cdot V \cdot N_C}{n_{Cell}} \cdot 100,$$

where Y is the product yield (%); C is the product concentration (mol L^{-1}); V is the reaction volume (L); M_C is

Table 3 Cellulose hydrolysis-dehydration in the presence of NbO_x/ZrO_2

Catalyst sample	pH of the reaction solution[a]		*R*, mol L^{-1} s^{-1} 10^6	TOF, s^{-1} 10^7	TOC, g L^{-1}	*X*, %	Yields of the products identified						
							Glu maximal[b]		Glu	5-HMF	Fr	FA	LA	Total
	Before	After					*Y*, %	*τ*, h	*Y*, %	*Y*, %	*Y*, %	*Y*, %	*Y*, %	Y_Σ, %
Blank	5.5	n.d.	0.2	–	n.d.	14.1	7.0	5	7.0	0.0	0.0	0.0	0.0	7.0
ZrO_2	4.5	2.7	2.3	2.8	2.16	50.0	12.7	3	12.6	13.3	0.0	0.5	0.0	26.4
0.5%Nb/ZrO_2	4.0	3.0	1.1	1.4	2.01	45.5	12.9	5	12.9	12.9	0.0	0.1	0.0	25.9
1.1%Nb/ZrO_2	3.6	2.8	4.0	4.8	2.26	52.3	21.3	3	17.9	16.3	0.0	0.0	1.8	36.0
2.8%Nb/ZrO_2	3.6	2.7	4.3	5.2	2.29	52.3	22.0	3	16.3	16.1	0.0	0.0	2.5	34.9

Conditions: [Cell]=[Cat] = 10 g L^{-1}, 45 mL, 453 K, P_{Ar} 10 bar, 1500 rpm, reaction time 5 h

Glu glucose, *Fr* fructose, *FA* formic acid, *LA* levulinic acid

[a]pH of the reaction solutions were measured before starting the experiment and after cooling down the reaction mixture at the end of test; pH of pure water is 5.5

[b]Maximal yield of glucose achieved during the experiment and the time of its achieving

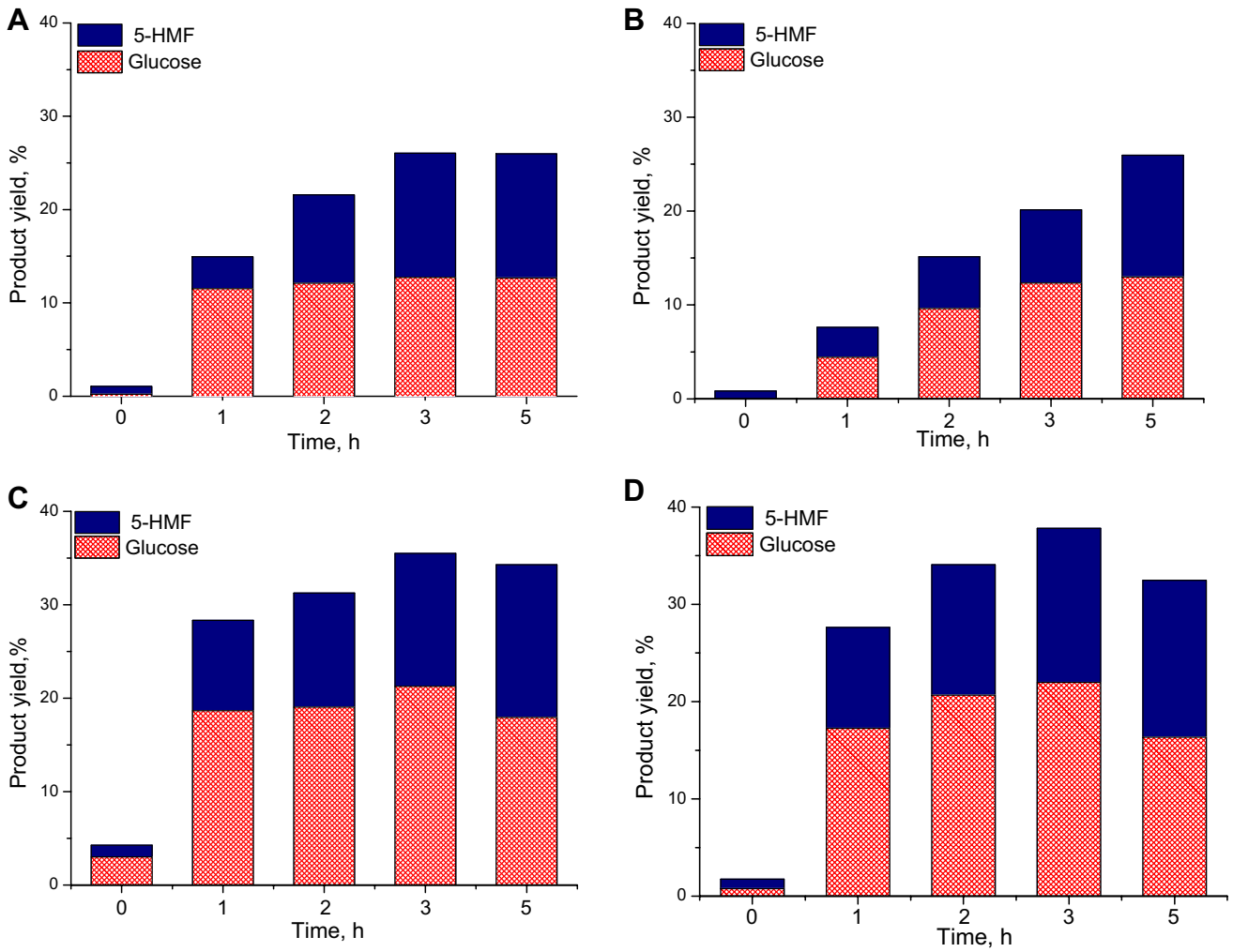

Fig. 4 The glucose and 5-HMF yields derived from cellulose versus reaction time in the presence of a catalyst (**a** ZrO_2; **b** 0.5%Nb/ZrO_2; **c** 1.1%Nb/ZrO_2; **d** 2.8%Nb/ZrO_2). Conditions: see Table 3

molar mass of carbon (g mol^{-1}); N_C is the number of carbon atoms in one product molecule (six in glucose, fructose and mannose, five in 5-HMF, furfural etc.); n_{Cell} is moles of carbon in cellulose sample (mol).

Turnover frequency, TOF (s^{-1}), i.e. the total amount of glucose and 5-HMF (mol) produced by Nb atoms and ZrO_2 of the catalysts (mol) per second was calculated according to formula:

$$TOF = \frac{R \cdot V}{m_{cat} \cdot \left(\frac{\omega_{Nb}}{M_{Nb}} + \frac{\omega_{ZrO_2}}{M_{ZrO_2}} \right)},$$

where R is the initial rate of glucose and 5-HMF formation (mol L^{-1} s^{-1}); V is the volume of the reaction mixture (L); m_{cat} is the catalyst mass (g); M_{Nb} is the molar mass of niobium (g mol^{-1}); M_{ZrO_2} is the molar mass of zirconia (g mol^{-1}); ω_{Nb} and ω_{ZrO_2} are mass fractions of niobium and zirconia, respectively.

The initial reaction rate (R) was determined from the kinetic data as follows:

$$R = \frac{(C_{Glu} + C_{5-HMF}) - (C^0{}_{Glu} + C^0{}_{5-HMF})}{\tau},$$

where R is the rate of glucose and 5-HMF formation (mol L^{-1} s^{-1}); C_{Glu} and C_{5-HMF} are concentrations of glucose and 5-HMF (mol L^{-1}), respectively, achieved at the second kinetic point (1 h); C^0_{Glu} and C^0_{5-HMF} are the concentrations of glucose and 5-HMF (mol L^{-1}), respectively, at the first kinetic point (0 h); τ is the reaction time measured in seconds (3600 s).

Maximum yields of all the side products usually were no more than 1–1.5 mol% except the yield of levulinic acid that reached 1.8 and 2.5 mol% in 5 h of the reaction over 1.1%Nb/ZrO_2 and 2.8%Nb/ZrO_2, respectively (Table 3).

All the catalysts were highly active to the formation of 5-HMF, while it was not formed in the blank experiment at all. In the blank experiment, the maximal glucose yield was no more than 7.0% in 5 h of the reaction. In the presence of all the solid catalyst under study the cellulose conversion was around 50% and glucose yields were 12–22%. Hence, our catalysts interact indeed with cellulose and catalyze its depolymerization probably by the acid mediated mechanism. Inspection of pH of the reaction solution also showed the increasing activity. pH varied in the range of 3.6–4.5 in the presence of the catalysts. An increase in the Nb amount leads to a rise of pH compared to pure ZrO_2.

Initial reaction rates (R) calculated from combined kinetics of glucose and 5-HMF formation are 5–20 times higher in the presence of the catalysts compared to the blank experiment. The activity of pure zirconia (without Nb) was high enough. Maximum yields of glucose and 5-HMF over ZrO_2 were 12.7 and 13.3 mol%, respectively. The observed activity of this catalyst to cellulose treatment was higher than that described in literature. Wang and co-authors reported 9 mol% glucose yield and 15.8 mol% total yield from cellulose over pure ZrO_2 after 12 h at 433 K [33]. The activity of pure ZrO_2 prepared by us also is comparable to the activity of mixed ZrO_2–TiO_2 (8.6 mol% 5-HMF yield at 573 K [46]) and sulfated ZrO_2 (14 mol% of glucose at 423 K and 24 h [32]).

However, almost two-fold decrease in the catalytic activity (initial reaction rate R and TOF) was observed upon addition of a small amount of NbO_x into the catalyst. The close yield of glucose (12.9 mol%) was only reached at 5 h of the reaction (Fig. 4a, b). The activity of 0.5%Nb/ZrO_2 decreased even though the acidity of the reaction solution increased compared to that of ZrO_2. The further increase in the Nb loading upto 1.1 and 2.8 wt.% led to ca. two times increase in the activity against that observed with ZrO_2. Close activities of 1.1%Nb/ZrO_2 and 2.8%Nb/ZrO_2 and close yields of glucose and 5-HMF over these catalysts (21–22 and 16 mol%, respectively, see Table 3; Fig. 4c, d) were revealed. However the yield of levulinic acid formed via 5-HMF decomposition was somewhat higher over 2.8%Nb/ZrO_2 than over 1.1%Nb/ZrO_2 indicating that the catalytic activity of 2.8%Nb/ZrO_2 was a little bit higher. These similar results can be accounted for by close pH of the reaction media in spite of more than twofold difference in the Nb loading.

To our knowledge, the NbO_x/ZrO_2 catalytic system was not been used before for direct cellulose transformation to glucose and 5-HMF in pure water. The application of niobium for cellulose depolymerization was studied by Takagaki et al. [75]; they used the $HNbMoO_6$ catalyst and observed the 1 mol% of glucose and a total 8.5 mol% yield of the main products (cellobiose and glucose). The authors assign the negligible yields of monomers and the absence of 5-HMF in the reaction products to the reaction temperature (373 K).

The activity changes can be interpreted in the following manner. Zirconia is known to be an acid-base bifunctional catalyst, and the cooperation of weak Lewis acid and weak base sites (acid-base pairs are suitably oriented on ZrO_2) plays an important role in the achievement of high selectivity to some reactions [76]. The concentration of Lewis acid sites on the zirconia surface was shown not to decrease when niobium oxide was supported on the surface [54]. We referred to the literature data in assuming that, in spite of slightly increasing total acidity (according to pH) of the reaction medium, the activity of 0.5%Nb/ZrO_2 decreases against that of ZrO_2 due to the formation of dispersed isolated NbO_4 species (40% of monolayer) to isolate spatially the acid and base centers (according to UV–vis DRS). This also allowed us to suppose that the catalyst surface plays an important

role in the hydrolysis of cellulose to glucose. Unfortunately, as mentioned in Sect. 3.2, the direct techniques for measuring acidity (NH_3 or pyridine adsorption) are unsuitable for our catalysts because of the low Nb content and low surface area of the catalysts [67]. The formation of additional Brønsted sites was observed upon supporting niobium at the concentrations higher then 0.69, 3.4 and 5 wt.% on zirconia [54], titania [77], and alumina [78], respectively. Analysis of the Nb phase structure showed that the Brønsted acidity was caused by polymer NbO_x species, while the isolated species had no acidity [54]. In the catalysts under study, the formation of polymerized NbO_x (NbO_6) species was observed (see UV–Vis DRS data above) in the samples containing 1.1 and 2.8 wt.% Nb at a more than monolayer Nb coverage. Obviously, additional acid sites are responsible for the increasing activity to cellulose depolymerization.

After completing the reaction, the TOC concentration in the reaction solutions was analyzed (Table 3). TOC values appeared quite close to one another and increased as follows: $2.01 < 2.16 < 2.26 \sim 2.29$ g L^{-1}. This series is similar to the series of the catalyst activity 0.5%Nb/$ZrO_2 < ZrO_2 << 1.1\%Nb/ZrO_2 \sim 2.8\%Nb/ZrO_2$. The cellulose conversion (X) was calculated from the TOC data by the following formula (Table 3):

$$X_{Cell} = \frac{C_C \cdot V}{m_{Cell}} \cdot 100,$$

where X_{Cell} is cellulose conversion (%); C_C is the concentration of carbon atoms (g L^{-1}); V is the reaction volume (L); m_{Cell} is the amount of carbon in cellulose sample (g).

The cellulose conversion was 14.1% in the blank experiment but close to 50% in all catalytic experiments. The highest conversion equal to 52.3% was observed over 1.1%Nb/ZrO_2 and 2.8%Nb/ZrO_2.

3.4 Hydrothermal Transformation of Monosaccharides and 5-HMF

The most active catalyst 2.8%Nb/ZrO_2 was tested in dehydration of main intermediates of cellulose transformation (glucose and fructose) and in degradation of 5-HMF under conditions identical to the cellulose treatment (Table 4; Fig. 5).

The initial reaction rate (R) was calculated as the rate of the substrate consumption:

$$R = -(C - C^0) \cdot \tau^{-1},$$

where R is the rate of glucose and 5-HMF formation (mol L^{-1} s^{-1}); C and C^0 are actual and initial concentrations of the substrate, respectively (mol L^{-1}); τ is the reaction time in seconds (3600 s).

The highest yields of 5-HMF obtained from glucose and fructose equal to 22.6 and 31.8 mol%, respectively were achieved in 3 and 0.5 h of the reaction. The fructose dehydration is a fast reaction (X of fructose was 100% in 1 h). Glucose transformation is much slower because it limited by isomerization of glucose to fructose. We did not achieved a very high yield of 5-HMF from monosaccharides due to its degradation (X = 56.7 mol% in 5 h) at 453 K. Lowering of the reaction temperature is expected to result in an increase in the yields of 5-HMF from the monosaccharides. The yields of levulinic and formic acids obtained from 5-HMF and furfural were very low in all the experiments.

4 Conclusions

A series of new Nb-containing zirconia catalysts were prepared, characterized (XRD, N_2 adsorption, ICP-OES, UV–Vis DRS) and tested for the first time in pure hot water in one–pot hydrolysis-dehydration of activated microcrystal

Table 4 Dehydration of the main cellulose transformation intermediates in the presence of 2.8%Nb/ZrO_2

Substrate	pH of the reaction solution[a]		R, mol L^{-1} s^{-1} 10^6	TOF, s^{-1} 10^7	X, %	Yields of the products						
						5-HMF maximum[b]		Glu	Fr	5-HMF	FA	LA
	Before	After				Y, %	τ, h	Y, %	Y, %	Y, %	Y, %	Y, %
Glucose	3.6	2.7	5.0	6.3	84.3	22.6	3	–	2.7	20.6	1.4	2.4
Fructose	3.6	2.7	9.4	11.8	100.0	31.8	0.5	16.4	–	10.5	3.2	8.2
5-HMF	3.6	2.7	1.0	0.1	56.7	–	–	0.0	0.0	–	2.2	4.2

Conditions: [Cat] = 10 g L^{-1}, [Substrate] = 50 mM L^{-1}, 45 mL, 453 K, P_{Ar} 10 bar, 1500 rpm, reaction time 5 h

Glu glucose, *Fr* fructose, *FA* formic acid, *LA* levulinic acid. Initial reaction rate (R), turnover frequency (*TOF*) and substrate conversion (X)

[a]pH of the reaction solutions were measured before starting the experiment and after cooling down the reaction mixture at the end of test; pH of pure water is 5.5

[b]Maximum yield achieved of 5-HMF during the experiment and the time of its achieving

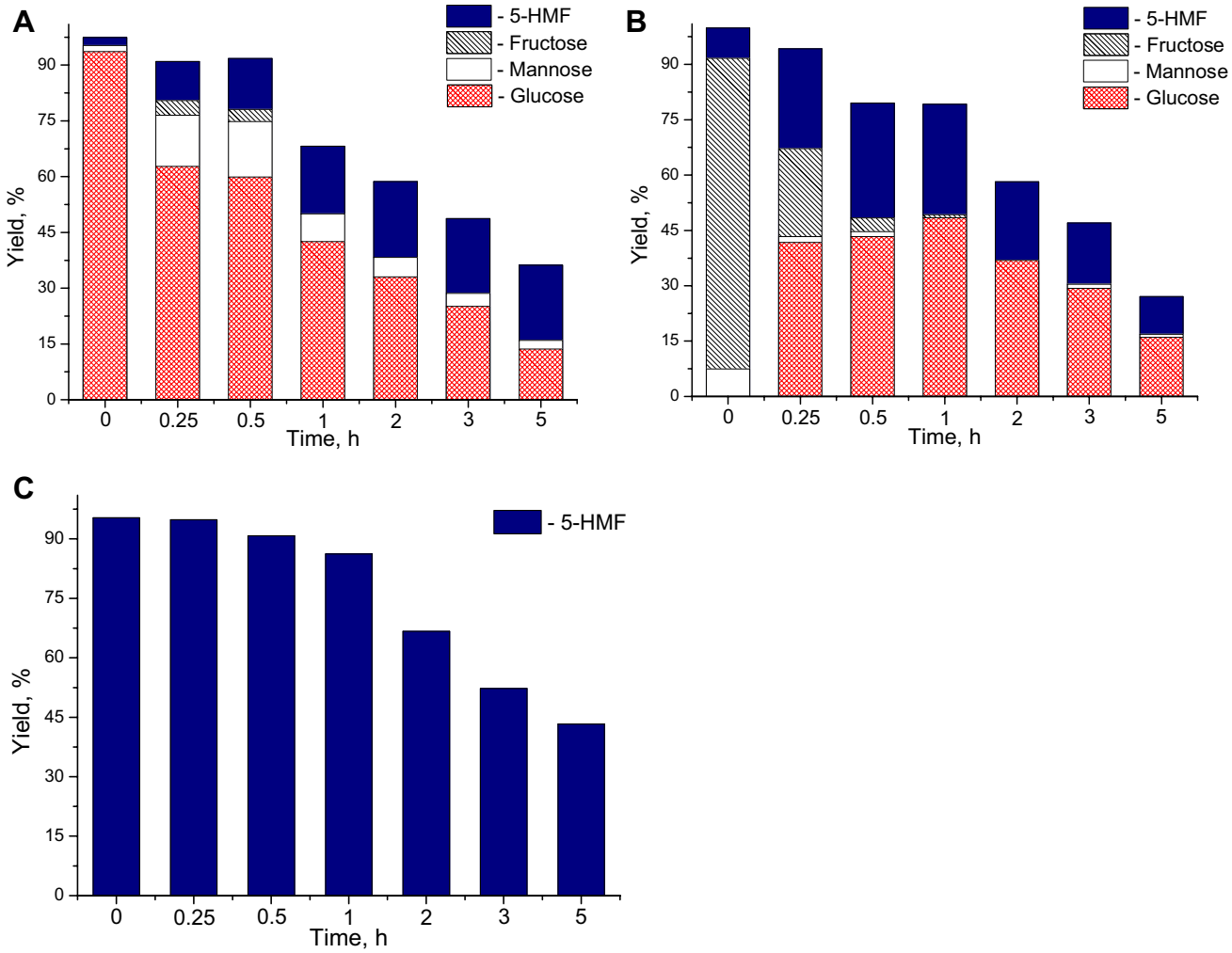

Fig. 5 The yields of glucose, mannose, fructose, and 5-HMF derived from glucose (**a**), fructose (**b**), and 5-HMF (**c**) versus time over 2.8%Nb/ZrO_2. Conditions: see Table 4

cellulose to produce glucose and 5-hydroxymethylfurfural. ICP-OES analysis of the spent catalysts and reaction solutions showed the excellent stability of the catalysts under hydrothermal conditions. The activity of the catalysts increased as follows: 0.5%Nb/ZrO_2 < ZrO_2 << 1.1%Nb/ZrO_2 ~ 2.8%Nb/ZrO_2. The maximum yields of glucose and 5-HMF were 22 and 16 mol%, respectively. All the catalysts were non-macroporous bulk zirconia containing mainly monoclinic phase of ZrO_2 (97–99%). The formation of Nb_2O_5 crystal phase was not observed. The state of NbO_x species was studied by UV–Vis DRS spectroscopy. 0.5%Nb/ZrO_2 contained niobium as inactive isolated NbO_4 species, while polymerized niobium oxide NbO_x (NbO_6) resided on the surface of 1.1%Nb/ZrO_2 and 2.8%Nb/ZrO_2. Isolated NbO_4 structures separated acid and base sites of ZrO_2 to decrease its own catalyst activity. Polymeric niobium oxide bore Brønsted acid sites, thus increasing essentially the acid properties and the catalytic activity.

Acknowledgements The authors are grateful to Dr. Artem B. Ayupov for N_2 adsorption measurements, Dr. Tatiana Yu. Kardash for XRD studies and Dr. Nina A. Rudina for SEM analysis. This work was supported by Russian Academy of Sciences and Federal Agency of Scientific Organizations as well as the Russian Foundation for Basic Researches (Grant 17-03-01142_a).

References

1. van Putten R-J, van der Waal JC, de Jong E, Rasrendra CB, Heeres HJ, de Vries JG (2013) Chem Rev 113:1499–1597
2. van de Vyver S, Geboers J, Jacobs PA, Sels BF (2011) ChemCatChem 3:82–94
3. Mäki-Arvela P, Simakova IL, Salmi T, Murzin DY (2014) Chem Rev 114:1909–1971
4. Besson M, Gallezot P, Pinel C (2014) Chem Rev 114:1827–1870
5. Dusselier M, Mascal M, Sels BF (2014) In: Nicholas KM (ed) Selective catalysis for renewable feedstocks and chemicals. Springer International Publishing, Cham, &, pp 1–40
6. Gallezot P (2012) Chem Soc Rev 41:1538–1558

7. Delidovich I, Leonhard K, Palkovits R (2014) Energy Env Sci 7:2803–2830
8. Bhaumik P, Dhepe PL (2016) Catal Rev s58:36–112ss
9. Chatterjee C, Pong F, Sen A (2015) Green Chem 17:40–71
10. Zhang ZC (2013) In: Suib SL (ed) New and future developments in catalysis. Elsevier, Amsterdam, pp 53–71
11. Tong X, Ma Y, Li Y (2010) Appl Catal A 385:1–13
12. Xue Z, Ma M-G, Li Z, Mu T (2016) RSC Adv 6:98874–98892
13. Teong SP, Yi G, Zhang Y (2014) Green Chem 16:2015–2026
14. Roman-Leshkov Y, Chheda JN, Dumesic JA (2006) Science 312:1933
15. Corma A, Iborra S, Velty A (2007) Chem Rev 107:2411–2502
16. Román-Leshkov Y, Dumesic JA (2009) Top Catal 52:297–303
17. Chheda JN, Roman-Leshkov Y, Dumesic JA (2007) Green Chem 9:342–350
18. Román-Leshkov Y, Chheda JN, Dumesic JA (2006) Science 312:1933–1937
19. Xu S, Yan X, Bu Q, Xia H (2016) RSC Adv 6:8048–8052
20. Bhaumik P, Dhepe PL (2013) RSC Adv 3:17156–17165
21. Tong X, Ma Y, Li Y (2010) Carbohydr Res 345:1698
22. Moreau C, Finiels A, Vanoye L (2006) J Mol Catal A 253:165
23. Fang Z, Liu B, Luo J, Ren Y, Zhang Z (2014) Biomass Bioenergy 60:171–177
24. Krawielitzki S, Kläusli TM (2015) Ind Biotechnol 11:6–8
25. http://www.ava-biochem.com/pages/en/products/5-hmf/description.php. Accessed 21 Apr 2017
26. Heinze T (2005) Polysaccharides. In: Dumitriu S (ed) Structural diversity and functional versatility, 2nd edn. Marcel Dekker, New York, p 551
27. Zhou P, Zhang Z (2016) Catal Sci Technol 6:3694–3712
28. Soldi V (2005) Polysaccharides. In: In:s Dimitriu S (ed) Structural diversity and functional versatility, 2nd edn. Marcel Dekker, New York, pp 395–406
29. Shimizu K-I, Furukawa H, Kobayashi N, Itaya Y, Satsuma A (2009) Green Chem 11:1627–1632
30. Pang J, Wang A, Zheng M, Zhang T (2010) Chem Comm 46:6935–6937
31. Kobayashi H, Komanoya T, Hara K, Fukuoka A (2010) ChemSusChem 3:440–443
32. Onda A, Ochi T, Yanagisawa K (2008) Green Chem 10:1033–1037
33. Wang H, Zhang C, He H, Wang L (2012) J Env Sci 24:473–478
34. Dhepe PL, Fukuoka A (2008) ChemSusChem 1:969–975
35. Dhepe PL, Ohashi M, Inagaki S, Ichikawa M, Fukuoka A (2005) Catal Lett 102:163–169
36. Nandiwale KY, Galande ND, Thakur P, Sawant SD, Zambre VP, Bokade VV (2014) ACS Sustain Chem Eng 2:1928–1932
37. Okuhara T (2002) Chem Rev 102:3641–3666
38. Marzo M, Gervasini A, Carniti P (2012) Carbohydr Res 347:23–31
39. Tagusagawa C, Takagaki A, Iguchi A, Takanabe K, Kondo JN, Ebitani K (2010) Angew Chem Int 49:1128–1132
40. Kourieh R, Bennici S, Marzo M, Gervasini A, Auroux A (2012) Catal Comm 19:119–126
41. Yan H, Yang Y, Tong D, Xiang X, Hu C (2009) Catal Comm 10:1558–1563
42. Carniti P, Gervasini A, Biella S, Auroux A (2006) Catal Today 118:373–378
43. Qi X, Watanabe M, Aida TM, Smith Jr RL (2008) Catal Comm 9:2244
44. Kitano M, Nakajima K, Kondo JN, Hayashi S, Hara M (2010) J Am Chem Soc 132:6622–6623
45. Watanabe M, Aizawa Y, Iida T, Nishimura R, Inomata H (2005) Appl Catal A 295:150–156
46. Chareonlimkun A, Champreda V, Shotipruk A et al (2010) Bioresour Technol 101:4179–4186
47. Hu L, Lin L, Wu Z, Zhou S, Liu S (2015) Appl Catal B 174–175:225–243
48. Gliozzi G, Innorta A, Mancini A, Bortolo R, Perego C, Ricci M, Cavani F (2014) Appl Catal B 145:24–33
49. Onda A, Ochi T, Yanagisawa K (2009) Top Catal 52:801–807
50. Chareonlimkun A, Champreda V, Shotipruk A, Laosiripojana N (2010) Fuel 89:2873–2880
51. Lai D-m, Deng L, Li J, Liao B, Guo Q-x, Fu Y (2011) ChemSusChem 4:55–58
52. Tanabe K (2003) Catal Today 78:65–77
53. Yang F, Liu Q, Bai X, Du Y (2011) Bioresour Technol 102:3424–3429
54. Onfroy T, Clet G, Houalla M (2005) J Phys Chem B 109:14588–14594
55. Lauriol-Garbey P, Millet JMM, Loridant S, Bellière-Baca V, Rey P (2011) J Catal 281:362–370
56. Peng G, Wang X, Chen X, Jiang Y, Mu X (2014) J Ind Eng Chem 20:2641–2645
57. Tauc J, Grigorovici R, Vancu A (1966) Phys Status Solidi B 15:627–637
58. Sewalt VJH, Glasser WG, Fontenot JP (1992) Animal Sci Res Rep Virginia Agric Exp Station 10:111
59. Park S, Baker JO, Himmel ME, Parilla PA, Johnson DK (2010) Biotechnol Fuels 3:s10
60. Scherrer P (1918) Nachrichten von der Gesellschaft der Wissenschaften zu Göttingen 1918:98–100
61. Mosier N, Wyman C, Dale B, Elander R, Lee YY, Holtzapple M, Ladisch M (2005) Bioresour Technol 96:673–686
62. Zhao H, Kwak JH, Wang Y, Franz JA, White JM, Holladay JE (2006) Energy Fuels 20:807–811
63. Mazeau K, Heux L (2003) J Phys Chem B 107:2394–2403
64. Yang P, Kobatashi N, Fukuoka A (2011) Chin J Catal 32:716–722
65. Jehng J-M, Wachs IE (1991) J Mol Catal 67:369–387
66. Mestres L, Martínez-Sarrión ML, Castaño O, Fernández-Urbán J (2001) Zeitschrift für anorganische allgemeine Chemie 627:294–298
67. Datka J, Turek AM, Jehng JM, Wachs IE (1992) J Catal 135:186–199
68. Gao X, Wachs IE, Wong MS, Ying JY (2001) J Catal 203:18–24
69. Klinger D, Vogel H (2010) J Supercrit Fluids 55:259–270
70. Sasaki M, Kabyemela B, Malaluan R, Hirose S, Takeda N, Adschiri T, Arai K (1998) J Supercrit Fluids 13:261–268
71. Bobleter O (2005) Polysaccharides. In: Dimitriu S (ed) Structural diversity and functional versatility, 2nd edn. Marcel Dekker, New York, pp 893–913
72. Marshall WL, Franck EU (1981) J Phys Chem Ref Data 10:295–304
73. Chandler K, Deng F, Dillow AK, Liotta CL, Eckert CA (1997) Ind Eng Chem Res 36:5175–5179
74. Romero A, Alonso E, Sastre Á, Nieto-Márquez A (2016) Microporous Mesoporous Mater 224:1–8
75. Takagaki A, Tagusagawa C, Domen K (2008) Chem Comm 2008:5363–5365
76. Tanabe K, Yamaguchi T (1994) Catal Today 20:185–198
77. Prasetyssoko D, Ramli Z, Endud S, Nur H (2008) Adv Mater Sci Eng 2008:345895
78. Tanaka T, Nojima H, Yoshida H, Nakagawa H, Funabiki T, Yoshida S (1993) Catal Today 16:297–307